JOURNAL OF SOLID STATE CHEMISTRY 106, 35–47 (1993)

Structures and Stabilization Mechanisms in Chemically Stabilized Ceramics

PRATIBHA L. GAI-BOYES*,†, MICHAEL A. SALTZBERG, AND ALEXANDER VEGA

Central Research and Development Department, DuPont Science and Engineering Laboratories, Experimental Station, Wilmington Delaware 19880-0356

Received December 4, 1992; accepted December 23, 1992

IN HONOR OF SIR JOHN MEURIG THOMAS ON HIS 60TH BIRTHDAY

Structural complexities and disorder in chemically stabilized cristobalites (CSC), which are room temperature silica-based ceramics, prepared by a wet chemical route, are described. CSC displays many of the structural characteristics of the high temperature cristobalite, elucidated by HREM and X-ray diffraction. *In-situ* electron diffraction and NMR results suggest that the disorder is structural and is static. © 1993 Academic Press, Inc.

Preface

I have been immensely privileged to work with Professor Sir John Meurig Thomas, FRS. I came to know him first through Professor J. S. Anderson, FRS. I have maintained a very rewarding collaboration with him over the years on advanced materials and benefitted by his insights, for which I am deeply indebted to him. Sir John has been a pioneer in the applications of high resolution electron microscopy (HREM) to solid state chemistry, for direct structural elucidation of grossly nonstoichiometric solids (*1*). He was the first to combine the structure imaging technique and simultaneous EDX microchemical analysis (*2*), with data from magic angle spinning NMR (*3*), to explore complex and new structures. His novel developments and ideas are continuing to contribute greatly to the fundamental understanding of complex oxides, zeolite catalysts, and silicate chemistry: important areas in which we all owe a tremendous debt to Sir John. Now all solid state scientists are using these techniques to unravel structural complexities. For this special issue in honor of Sir John, I have chosen a topic in which many of the techniques, concepts and elegant correlations he has pioneered, have been essential to gaining insights into structures and disorder in our preparations of chemically stabilized complex silica-based room temperature ceramics, some with novel compositions. The article is based on my seminar at the Royal Institution.

—Pratibha Gai-Boyes

Introduction

Structures based on networks of corner-shared tetrahedra of oxygen ions connected to a central cation are some of the most fundamental in crystal chemistry. Silica-based ceramics belong to such a class of compounds. The cristobalite form of silica has two modifications, α (low) and β (high), which are separated by a sudden displacive transition at ~270°C. This paper describes our structural studies of chemically stabilized cristobalite (CSC), a room temperature

* To whom correspondence should be addressed.

† (PLG-B is also at the Department of Chemical Engineering, (Materials Science), University of Delaware.)

0022-4596/93 $5.00

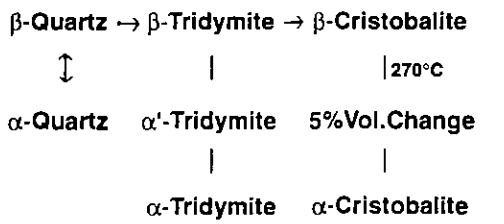

FIG. 1. Some common polymorphs of silica, which exhibit displacive phase transitions.

silica-based ceramic containing small amounts of dopants, prepared by a wet chemical route. It displays many of the structural characteristics of the high temperature β-cristobalite (*17*), but does not undergo phase inversion to α-cristobalite upon cooling.

Synthesis of stabilized "β-cristobalite-like phases" by other routes, e.g., solid state, or sol-gel routes, has been reported, but these yielded poorly crystallized, multiphasic ceramic materials (*4*). The relationship between various crystalline phases of silica has been studied extensively over the past century. The traditional view after Fenner (*5*), is that, there are three distinct families of silica structures stable at ambient pressure: quartz, tridymite, and cristobalite. Although quartz is believed to be the stable phase below 900°C, both tridymite and cristobalite can be cooled below this temperature where they are metastable. Upon cooling, each of the phases undergoes one or more $\beta \rightarrow \alpha$ type inversions. Fenner found that $\beta \rightarrow \alpha$ inversion in cristobalite varies from ~180–270°C, depending on the synthesis history of the sample. However, the phase relationship between the various forms of cristobalite and tridymite is more complex than previously believed, and is shown in Fig. 1. Pure silica never adopts the tridymite structure, which is formed only in the presence of impurities such as alkali ions.

Structural Considerations

Silica has several polymorphs: quartz, tridymite, coesite, stishovite, cristobalite, and (dealuminated Y-zeolite). The two of the commonest forms, cristobalite and tridymite, have tetrahedral framework structures, composed of layers of six-membered rings of $SiO_{4/2}$ tetrahedra. The stacking sequence of these layers in cristobalite is "cubic," *ABCABC*, while in tridymite it is hexagonal, *AB'AB'AB'* (*6*). Florke (*7*) postulated in a series of classic papers that tridymitic stacking faults caused by low crystallization temperature and/or impurity ions, lead to a lower $\alpha \rightarrow \beta$ phase transition temperature in cristobalite, and this was confirmed by others (*8*). Figures 2a, 2b, and 2c show structural schematics of α, idealized and disordered β phases, respectively (*9, 10*). The structure of α is well established (*11*): it is tetragonal, space group $P4_12_12$, with $a = 4.98$ Å and $c = 6.95$ Å. The structure of β is not yet completely understood (*10, 12*). The general consensus (*10, 11, 23*) suggests that the structure is cubic, space group $Fd3m$, and $a = 7.17$ Å. According to the hypothesis of Wright and Leadbetter (*10*), the oxygen atoms occupy the six 96(*h*) sites in $Fd3m$, which occur around the annulus as shown in Fig. 2c. Only one position of the six (*h*) positions on a circle around each 16(*c*) positions in the space group $Fd3m$ can be occupied at a time. The only plausible interpretation of this oxygen distribution is short range order in domains of lower symmetry, within each domain a subset of one sixth of the 96(*h*) sites being occupied and domains of each of the six possible subsets occurring with equal probability as suggested by O'Keefe and Hyde (*9*). The presence of diffuse scattering in β has been reported in the literature (*12*), and will be discussed in the following sections.

Previous work (*13*) explains the stabilization of the β-cristobalite-like phase as due to the "stuffing" concept, where the incorporation of the foreign ions in the interstices of silicate structures is charge-compenstated by the substitution of Al^{3+} for Si^{4+} in the framework. The presence of foreign ions in the interstices presumably inhibits the contraction of the structure normally oc-

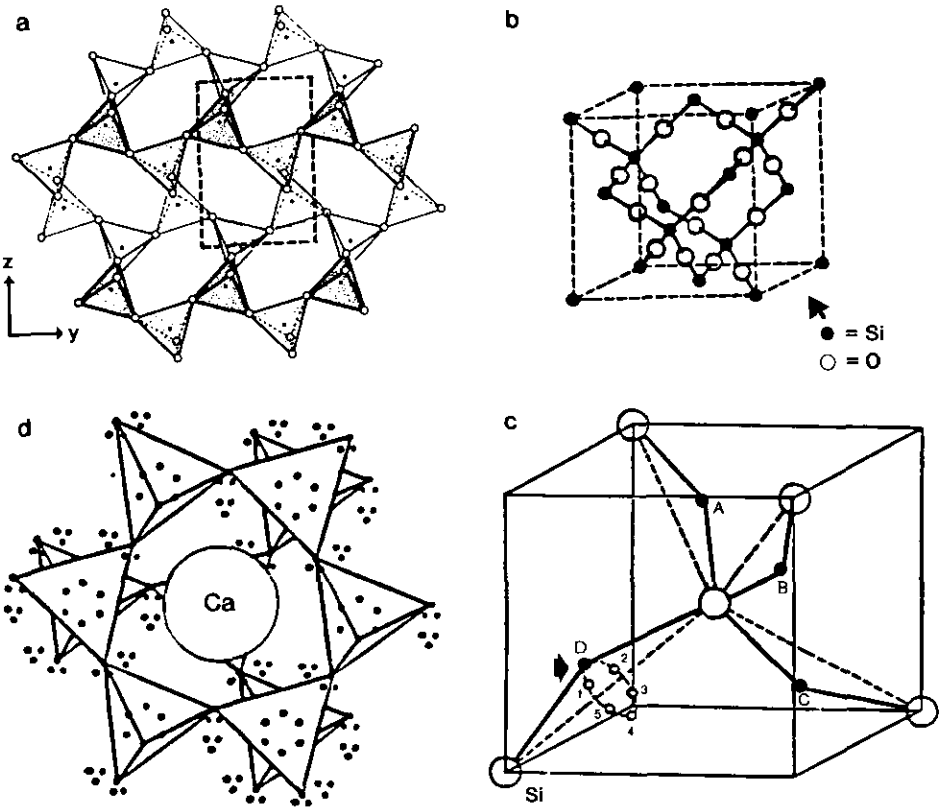

FIG. 2. (a) The structure of α-cristobalite in (100) projection (after O'Keefe and Hyde (1976)). (b) Idealized structure of β-cristobalite (high-cristobalite). (c) The local atomic arrangement, with a disordered domain structure in β, suggested by Wright and Leadbetter (1975). Large circles are Si atom-positions and small circles are oxygens. Only one of the six (h) positions on the annulus around each of the 16(c) in space group $Fd3m$ is thought to be occupied at a time. (d) Ca-ions residing in cages. Part of two layers of tetrahedra projected onto (111). (from Peacor (1973)).

curring in the $\beta \rightarrow \alpha$, thus stabilizing the β-cristobalite-like structure. It may be noted that Al can have both tetrahedral coordination as part of the basic silicate framework, and octahedral coordination as a charge compensating cation. Wilson *et al.* (*14*) described the X-ray data of a β-cristobalite-like phase found in certain silica minerals, by a structural model based on disordered α-tridymite. This model involves disorder within the layers of the six-membered rings themselves, rather than a simple disorder between well-defined layers. Following the NMR studies of silica polymorphs (*15*), Perrota *et al.* (*16*) report that the ^{29}Si NMR chemical shift of their stabilized β-cristobalite-like ceramics is closer to that of α-cristobalite, than to that of α-tridymite. The two structural models predict identical X-ray diffraction patterns; therefore, in the absence of electron diffraction data it is impossible to determine the microstructural variations of the stabilized β-cristobalite-like phase. Electron diffraction and HREM provide details of the ceramic microstructure and the extent of local ordering, and nuclear magnetic resonance spectroscopy (NMR) provides atomic level information about the environments of silicon atoms in the structure.

Since the true structure of these materials is unclear, we have chosen to call the

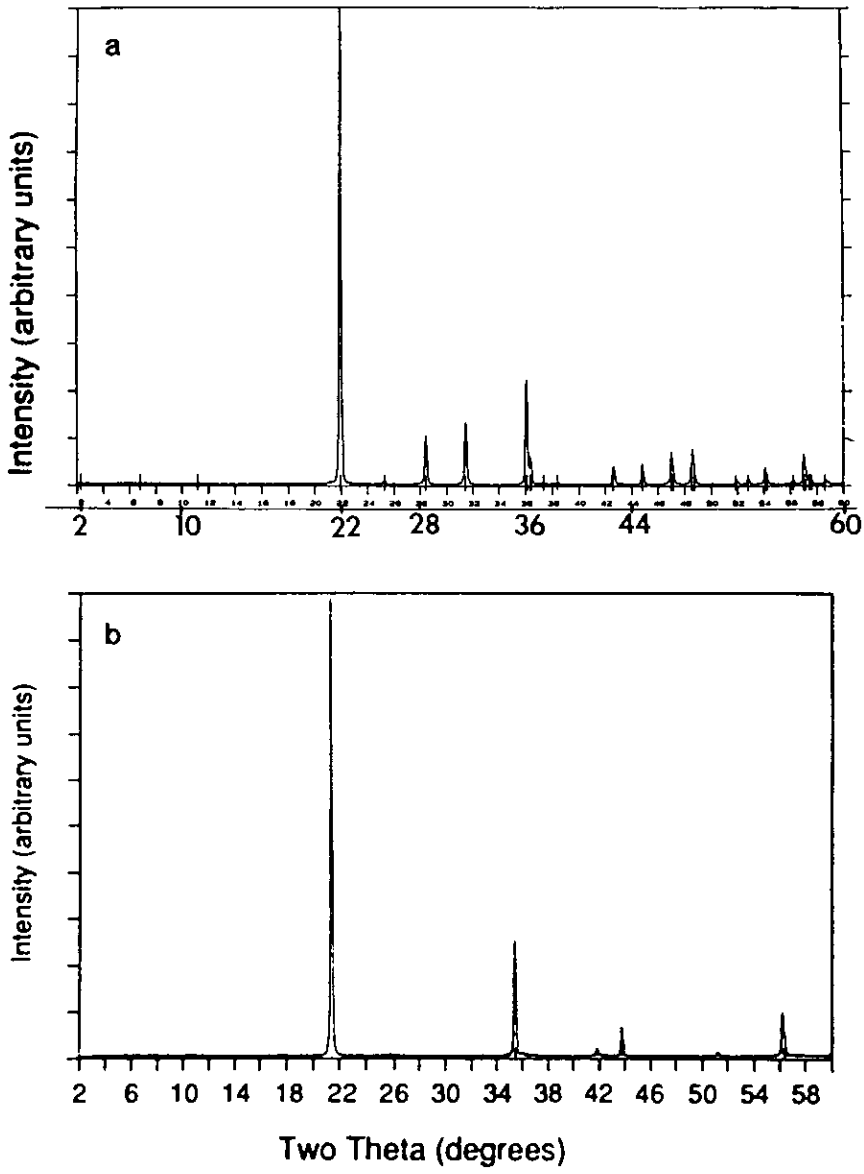

FIG. 3. X-ray diffraction patterns of (a) tetragonal α-cristobalite, and, (b) chemically stabilized room temperature cubic cristobalite (CSC). The sharp reflections in CSC indicate a well-crystallized, single phasic structure.

samples synthesized by our new route which do not undergo phase transformation, thus they are "stabilized," chemically stabilized cristobalite, or CSC.

Experimental Procedures

Compositions with varying Ca/Al ratio and substitutions in cristobalite have been described (*17*). For CSC, a clear sol was prepared from DuPont colloidal silica, Ludox AS-40, aluminum nitrate nonahydrate, and calcium nitrate hexahydrate in proportions to form a final composition 2.3 mole% CaO 4.7 Al_2O_3 93% SiO_2, i.e., 1 : 2 : 40 composition. This sol was spray-dried yielding an amorphous powder. This precursor was calcined at 1100°C for 24 hr to yield CSC.

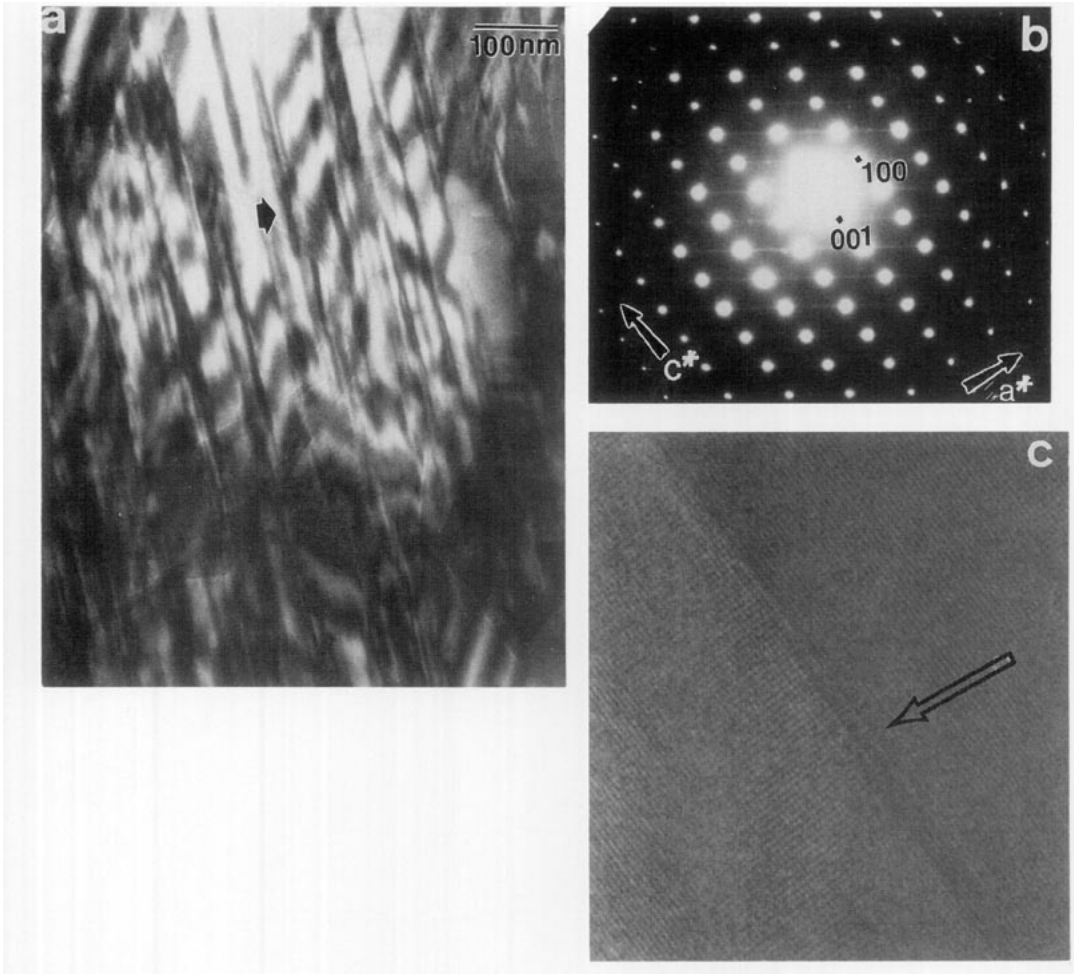

FIG. 4. Microstructure of α-cristobalite, (010) orientation: (a) a high concentration of stacking defects antiphase boundaries (APB) and twins along ⟨101⟩ directions, resulting from β–α phase inversion. (b) The corresponding electron diffraction pattern, with faint streaks due to the defects, along ⟨101⟩. (c) A lattice image of some of the defects in (101).

Well ordered α-cristobalite was prepared by crystallizing Aerosol, a very pure form of amorphous silica at 1400°C for 24 hr. Other compositions with varying Ca/Al in the series $CaO:Al_2O_3:SiO_2$ with the ratio $3\text{-}x : x : 40$ (with $x = 0$–3), and $CaO : 4Al_2O_3 : 40SiO_2$, $CaO : Al_2O_370SiO_2$ were also prepared with different calcination temperatures (1100, 1300, and 1500°C) and examined. Chemically stabilized compositions using transition metal (Cu), and alkali metal (K) were synthesized as above, in the systems $CuO : Al_2O_3 : SiO_2$ and $K_2O : Al_2O_3 : SiO_2$.

High resolution electron microscopy (HREM) and electron diffraction were performed using a CM30 supertwin HREM operating at 300 keV and fitted with a windowless EDX detector for simultaneous microcomposition analysis (*18*), and a CM 20 ultra twin HREM. To minimize atmospheric degradation, freshly prepared materials were used throughout. The samples were very sensitive under the electron beam, and imaging procedures used to minimize structural degradation for aluminosilicate zeolites, glass ceramics, and related phosphates

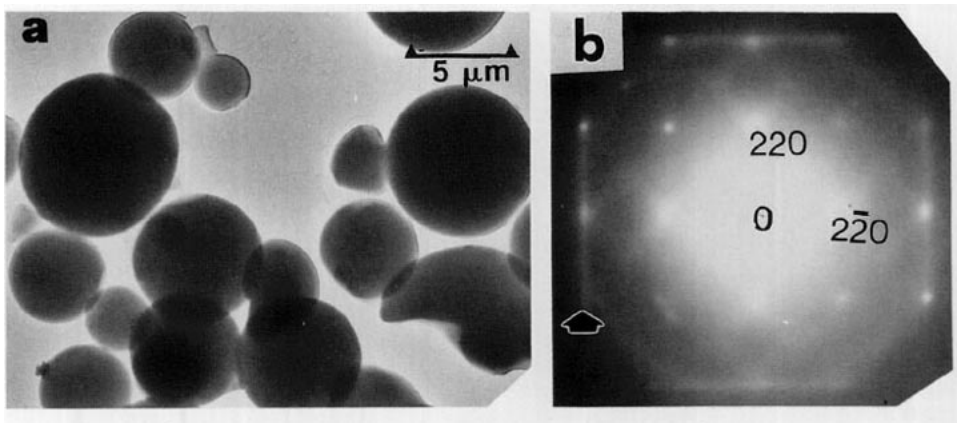

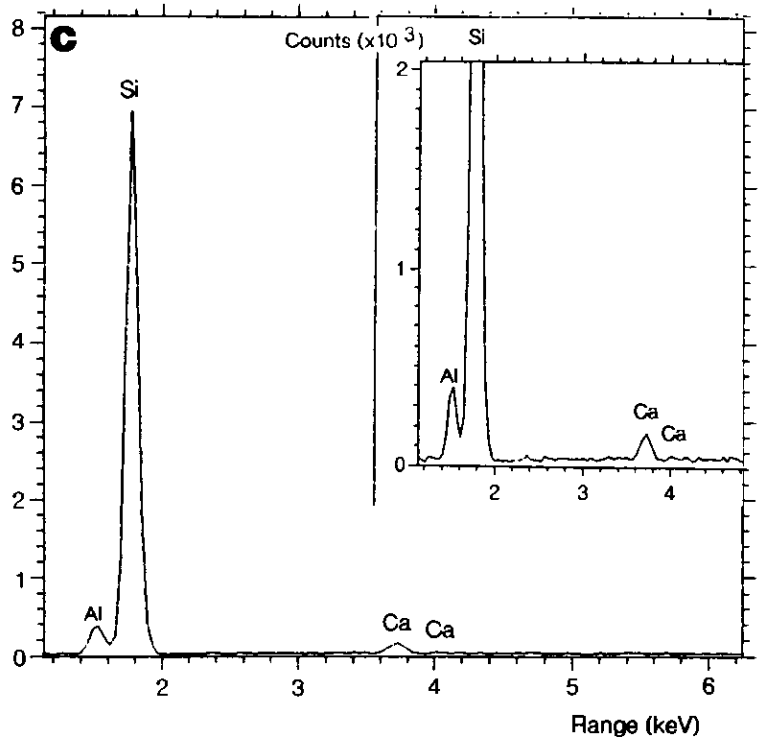

FIG. 5. Room temperature CSC ($CaO:2Al_2O_3:40SiO_2$): (a) microstructure; (c) composition (EDX) with Ca and Al incorporated into the structure; and (b) (001) electron diffraction (cubic) with complex diffuse streaking parallel to e.g. ⟨110⟩, ⟨100⟩. (d) HREM structure image of CSC (101) projection, indicating cubic symmetry. The chemical stabilization is characterized by the absence of faults, and by the absence of reversible phase transition observed in the high cristobalite. The regions of variable contrast (arrowed) may be attributed to disorder. (e) electron diffraction (inset) of (d), with streaks parallel to ⟨111⟩ and ⟨010⟩ directions.

were employed (*19–21*). The powders were supported on carbon-filmed copper or titanium grids. The small probe capability in the CM30 ST also allowed convergent beam electron diffraction facility providing structural information from a few nanometer regions. Samples were studied at room temperature (RT) and *in-situ* at elevated temperatures,

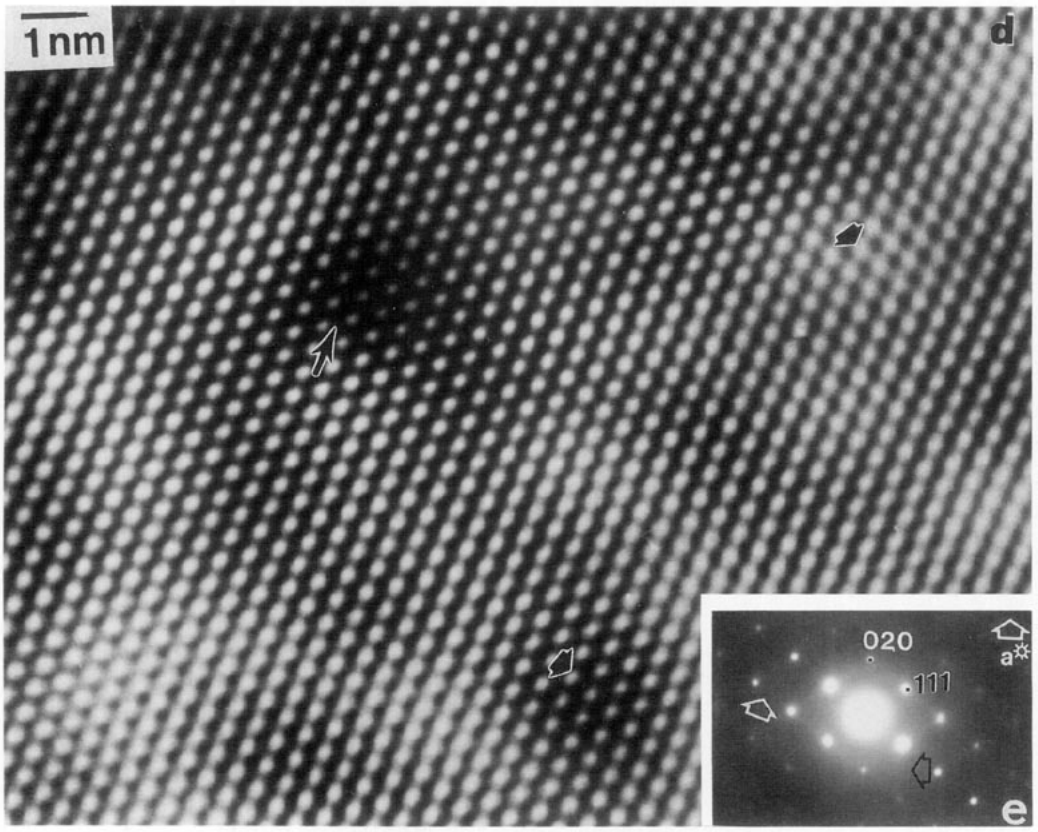

FIG. 5—*Continued*

using a hot stage, and at liquid nitrogen temperatures using a cold stage in this EM. The local structural changes were examined by electron diffraction, to provide insights into the microstructure, diffuse scattering and compositional changes. ^{29}Si signals were recorded using magic angle spinning (MAS) NMR, to provide information on the chemical bonding (Si–O–Si bond angles), aluminum distribution in the silica framework, and on secondary phases. The high temperature spectrum of the pure SiO_2-cristobalite was recorded for us by the NMR facility at Colorado State University.

Results

X-ray diffraction patterns of α-cristobalite and CSC are shown in Figs. 3a and 3b, respectively. The tetragonal reflections of α are absent in the CSC pattern, (as they are in the β-cristobalite phase). The reflections of the CSC are sharp, indicating a well-crystallized structure, in contrast to the relatively broad reflections observed in synthetic cristobalites and in natural cristobalitic opals reported in the literature.

Nanostructure and Microchemistry

Electron diffraction examinations reveal remarkable differences between the CSC and the undoped α-cristobalite. As shown in Fig. 4a, the local structure of undoped α-cristobalite in (010) projection reveals a high concentration of stacking defects, APBs and twins along ⟨101⟩ directions. These defects are probably introduced when the cubic β-cristobalite structure inverts to a tetragonal α-cristobalite upon cooling below 270°C

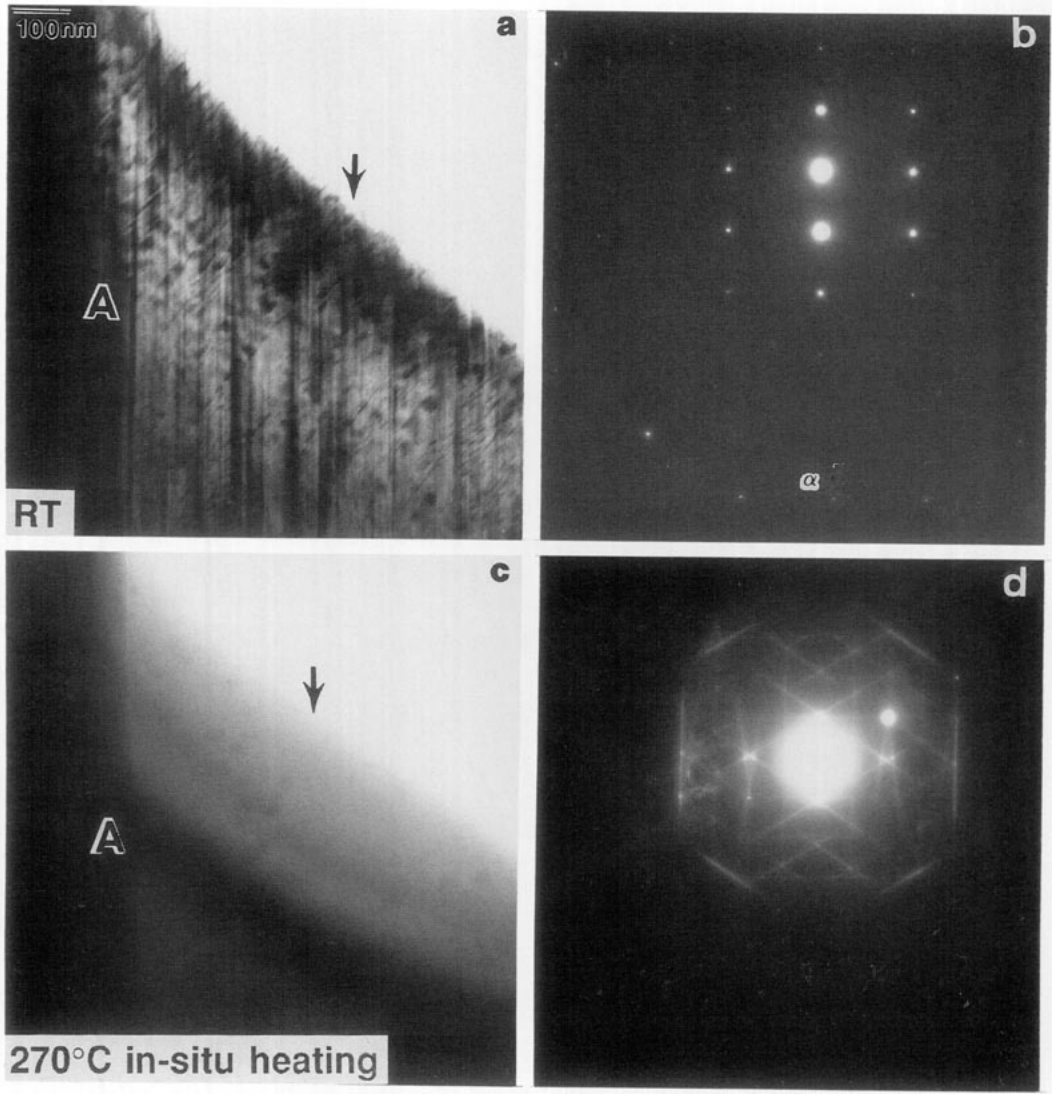

FIG. 6. *In-situ* electron microscopy experiments of α–β rapid phase inversion. The same area around A: (a) tetragonal pure α-cristobalite with stacking defects, APBs and twins at room temperature (RT) (b) electron diffraction pattern at RT; (c) sudden displacive transition to the β-phase at 270°C, (d) the corresponding electron diffraction (at 270°C), near the cubic [112] zone, with intense streaks. The directions of the streaks may be related to the lattice transformation direction. The streak intensities displayed no apparent change at higher temperatures.

(discussed in the next paragraph). The electron diffraction (b) shows faint streaks along ⟨101⟩ when the concentration of faults is high. A lattice image of a fault in (101) is shown in (c).

Microstructure of the room temperature CSC with the composition $CaO:2Al_2O_3:40SiO_2$ and the corresponding EDX spectrum indicating the incorporation of Ca and Al into the structure are shown in Figs. 5a and 5b, respectively. Electron diffraction patterns generally show complex and substantial diffuse scattering (Figs. 5b and 9). The HREM structure image of the CSC is

shown in Fig. 5d in (101) projection, indicating a cubic symmetry. The image also reveals small local deviations in contrast which are being examined. The chemical stabilization of the structure is characterized by the absence of faults or discernible extended defect structures, confirmed by careful tilting experiments in (101) and in other crystallographic orientations, as well as by dark field imaging and HREM (Fig. 5d). However, the corresponding electron diffraction shows diffuse streaks (Fig. 5e), with the streaks parallel to mainly ⟨111⟩ and ⟨010⟩ directions in this projection. The HREM image also reveals variable contrast (arrowed), which may be related to the diffuse scattering and disorder. The streaks are indicative of considerable disorder in the structure, to be discussed later. The electron diffraction data show that the structure is related to the high-cristobalite (see below). Further, these results are consistent with NMR data discussed in the following sections. CSC ceramics substituted with Cu and K exhibited similar behavior. These and other compositions with solid solution limits for the substitutions, will be reported elsewhere.

The rapid displacive transition between α and β has been studied directly, (*in situ*), using a hot stage in the CM30 EM: Figure 6a shows the room temperature α-cristobalite with stacking faults and twins, near area A, and (b) electron diffraction; (c) the same sample is heated *in situ* to 270°C, indicating a sudden phase transition to the β-phase. This is accompanied by the absence of the extended defect contrast (confirmed by tilting experiments), but by intense diffuse streaks in the electron diffraction pattern (shown in d, near the [112] zone axis). The streaks are parallel to the directions similar to those observed in the CSC samples. The diffuse scattering persisted at higher temperatures (~400°C) with little apparent change in intensities. This $\beta \rightarrow \alpha$ phase transition, which is reversible, is accompanied by 5% volume change, and is thus expected to disrupt the structure. CSC, which does not undergo any detectable phase transformation upon cooling, is essentially free of the stacking fault defects. The images in Fig. 5 also confirm that the "long-range" order of the CSC structure is maintained over at least 100 nm.

NMR

We report the NMR spectra for several $CaO : Al_2O_3 : SiO_2$ compositions and the results are shown in Figs. 7 and 8. Figure 7a shows the ^{29}Si spectra of α-cristobalite at room temperature, (b) the same sample in the β-form at 400°C, and (c) CSC of composition $CaO : Al_2O3 : SiO2 = 1 : 2 : 40$. All three spectra feature a peak in the vicinity of -110 ppm, but the exact chemical shifts and the line widths vary from sample to sample. The CSC spectrum shows, in addition, a broad shoulder around -105 ppm. Whereas the main peak arises from the Si atoms in the silica structure that are coordinated through oxygen bridges to four other silicon atoms, we believe that the shoulder is the signal of the Si atoms in the silica phase that are coordinated to one or two tetrahedral Al atoms in the silica framework. From zeolite work it is known that substitution of Si neighbor with Al results in a ^{29}Si peak shift over about $+5$ ppm (*22*). The relative intensity of this signal component is a measure of the concentration of tetrahedral Al. At low Al concentrations, the number of affected Si atoms is four times the number of tetrahedral Al sites. Although it is difficult to decompose the spectrum into two overlapping components, we estimate that the shoulder represents $20 \pm 5\%$ of the total signal intensity. Hence, the atomic ratio of tetrahedral Al and Si is close to 2 : 40, which is the level of the framework substitution expected for the case where each Ca^{2+} ion in the 1 : 2 : 40 composition resides in an interstitial site and serves as charge compensation for two tetrahedral Al atoms. Thus, the shoulder in the CSC spectrum is strong evidence for a high level Al substitution in the framework and consequently, a large number of Ca ions in the interstices, as shown schematically in Fig. 2d.

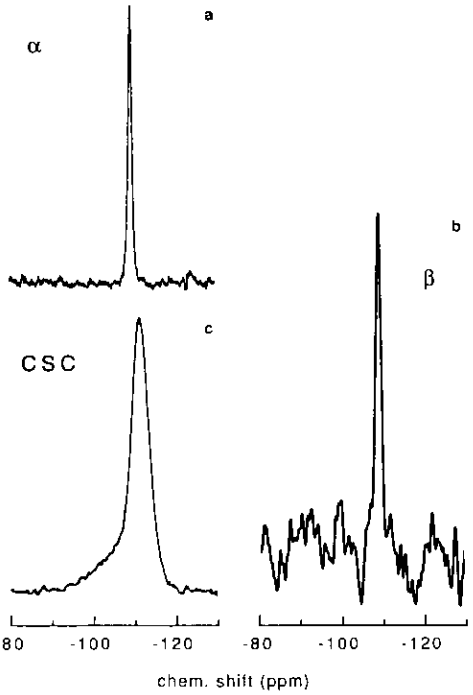

FIG. 7. ^{29}Si NMR spectra of: (a) α-cristobalite at room temperature; (b) The same sample in the β-form at 400°C; (c) CSC sample of composition $CaO:Al_2O_3:SiO_2 = 1:2:40$. The different chemical shifts and line widths are interpreted in the text.

The positions and the widths of the main silica peaks can be understood in terms of the well-established dependence of the chemical shift, δ, of a particular ^{29}Si nucleus on the average of the four surrounding Si–O–Si angles, $\langle\theta\rangle$. Various functional relationships between δ and $\langle\theta\rangle$ can be found in the literature describing this dependence. Since the numerical values predicted by these functions are essentially indistinguishable over the limited shift range presently encountered, we opt to analyze the spectra in Fig. 7, following the simplest of the models by Thomas *et al.* (*3*):

$$\delta(\text{ppm}) = -19.82 - 0.609\langle\theta\rangle(^\circ)$$

The peak maxima are at -108.9 for α-cristobalite at room temperature, -111.6 ppm for β-cristobalite at 400°C, and -111.7 ppm for CSC at room temperature, corresponding to average Si–O–Si bond angles of 146° in the α-form and 151° in CSC. The chemical shift of the 400°C sample might suggest that the bond angles in CSC are similar to those of undoped β-cristobalite. However, since we have no good reference for chemical shift measurements at high temperatures, it remains to be seen if this is a valid conclusion. Assuming that the Si–O bonds have approximately the same lengths in these phases, an increase in the bond angles leads to a more open framework structure and should thus be reflected in larger unit cell dimensions. Indeed the corresponding (101) d-spacings by XRD are 4.04 Å in the α-form and 4.079 Å in CSC.

Of particular interest is the width of distribution of Si–O–Si angles revealed by the width of the ^{29}Si spectra in Figs. 7 and 8. This type of information is not provided by XRD, as it does not reveal structural fluctuations on a length shorter than the coherence length of ~50 Å. NMR, on the other hand, gives a separate signal for each ^{29}Si nucleus. Hence the width of the resonance peak is a measure of structural fluctuations, i.e., structural disorder. The sharpness of the α-cristobalite peak confirms the uniformity of Si-environment in the ideal tetragonal crystal structure. The high-temperature spectrum is nearly as narrow as room-temperature spectrum. The full width half maximum (FWHM) of the spectrum of the β-

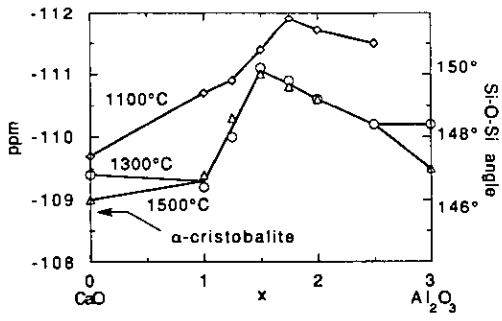

FIG. 8. Summary of ^{29}Si NMR chemical shifts and bond angles of the calcined samples with the composition $CaO:Al_2O_3:SiO_2 = (3-x):x:40$ (with $x = 0$ to 3).

form is 1.0 ppm (after correction for the artificial line broadening applied in the Fourier transform procedure), as compared to 0.9 ppm in the α-form. This suggests that the Si–O–Si angles are all equal to each other in the otherwise disordered β-structure, in agreement with Wright and Leadbetter's model of random but equidistant displacements of oxygen atoms from the centers of the Si–Si lines.

In contrast, the resonance of CSC is considerably broader, with a FWHM of 4.5 ppm, indicating a wide range of Si sites in the crystal structure (with an overall variation of average Si–O–Si angles between ~143 and ~159°). Since long-range order is ruled out by XRD, these fluctuation reflect short-range lattice deformations.

Figure 8 summarizes ^{29}Si NMR chemical shifts and Si–O–Si bond angles of the calcined samples in the composition $(3-x):x:40$ (with $x = 0$ to 3), at different temperatures. The maximum of the average Si–O–Si bond angles is ~151°.

Nature of Disorder and Role in Stabilization Mechanisms

The cause of the disorder and stabilization mechanisms in CSC is of considerable importance, since novel ceramics can be engineered by suitable stabilization procedures. Furthermore, the nature of the disorder, i.e., whether it is static (individual atoms frozen in one of a range of possible sites), or dynamic (each atom vibrating through a range of possible sites), requires some discussion. Here we discuss possible models:

HREM imaging (Fig. 5), tilting experiments and dark field imaging using the diffuse streaks, did not reveal any discernible extended defect structure contrast, ruling out shape effects. Using *in-situ* electron diffraction, we have therefore examined possible thermal diffuse scattering (TDS)/phonon scattering effects during heating and cooling of the CSC ceramics. In TDS, Bragg intensities depend critically on the Debye–Waller factors, which define the extent of thermal vibration of the atoms. TDS increases with increasing temperatures. Our preliminary experimental data are summarized in Fig. 9: Figs. 9a and 9b show electron diffraction data of CSC for room temperature (RT) and at −171°C. Figures 9d and 9e show the patterns at RT and 300°C. The patterns are close to (112), with streaks mainly parallel to ⟨111⟩ and ⟨110⟩ and ⟨102⟩ type directions, and the streaks do not appear to pass through the origin. The electron diffraction patterns were recorded under similar conditions of beam illumination, specimen tilt, and film exposure. Intensity profiles were recorded from the same streaks at different temperatures, some with a 5 μm objective aperture. Within experimental errors we find no significant difference in the streak intensities at various temperatures, which therefore rules out thermal vibrations. We emphasize, however, that quantitative intensity measurements are difficult to obtain from electron diffraction, since local tilt changes and multiple scattering effects may affect intensity distributions during heating.

Furthermore, the broadening of the NMR peak of CSC (Fig. 7c) implies that the fluctuation of Si–O–Si angles is static on the NMR scale. In other words, if the angles were fluctuating in time with a uniform average angle and with a characteristic time shorter than a millisecond, the ^{29}Si peak would become as narrow as in α-cristobalite. The observed distribution in the environment of Si atoms cannot thus be attributed to the thermal vibrations. A more plausible possibility is that they represent local static distortions caused by the incorporation of Ca and Al atoms in the crystal, the displacements being larger the closer the Si atom to an impurity site. The disorder is thus structural. However, NMR cannot determine if it is the positions of Si or oxygen that are displaced from their nominal sites.

Diffuse scattering in β has been investigated by lattice dynamical study and extensive Monte Carlo simulations (*12*). The rapidity of phase transition to α, accompanied

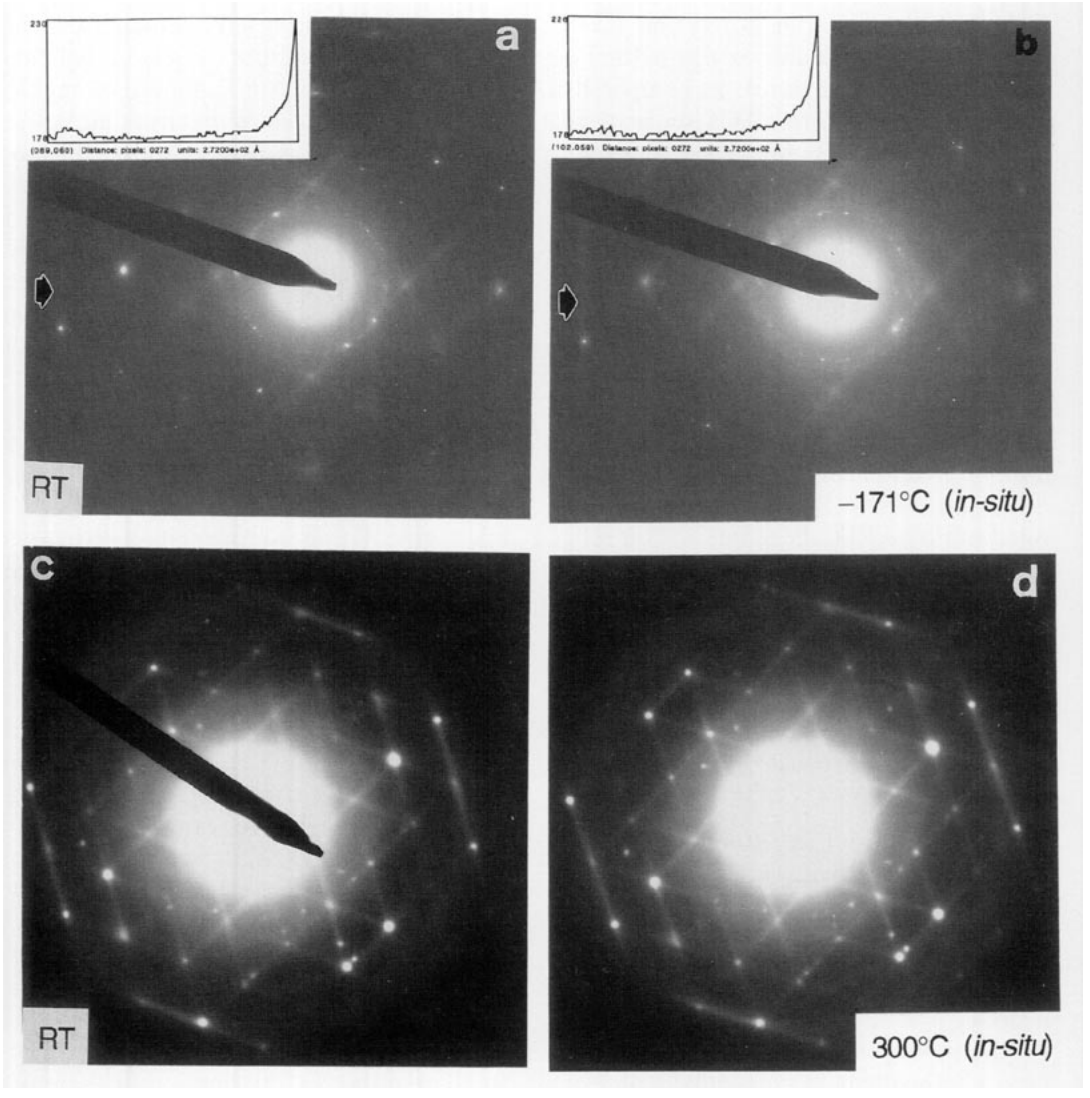

FIG. 9. *In-situ* electron diffraction of CSC from the same areas (a) RT, (b) −171°C, with insets of intensity line profiles from the streaks arrowed; (c) RT, (d) ~300°C. The diffuse streaks exhibit little apparent change at different temperatures. CSC does not undergo phase inversions.

by the sudden decrease in the diffuse intensity in experimental electron diffraction patterns (with diffuse planes normal to the six ⟨110⟩ directions of the $Fd3m$ cell), was thought to indicate TDS/phonon scattering in the study and the hypothesis of Wright and Leadbetter (*10*) was examined. However, there was no complete agreement between theory and experiment. As implied by the authors, single crystal neutron or X-ray diffraction studies would be worthwhile. Further, it may be noted that higher temperature experiments on β show no apparent change in diffuse intensities (as observed in the present study, and in Ref. (*12*)). It therefore remains to be seen whether the disorder in β is similar to the structural disorder we propose for the room temperature CSC.

Concluding Remarks

Structural complexities and disorder in chemically stabilized cristobalites (CSC), which are room temperature silica-based ce-

ramics, prepared by a wet chemical route, have been described. CSC displays many of the structural characteristics of the high cristobalite, elucidated by HREM and X-ray diffraction. *In-situ* electron diffraction and NMR results suggest that the disorder is structural and is static.

Acknowledgments

Pratibha Gai-Boyes thanks Professor C. N. R. Rao, FRS, for the kind invitation to prepare this article. We thank L. G. Hanna, S. C. Winchester, and R. O. Balback for technical assistance and the high temperature NMR facility at Colorado State University.

References

1. J. M. Thomas, *Philos. Trans. R. Soc. London A* **277,** 251 (1974).
2. J. M. Thomas, *Ultramicroscopy* **8,** 13 (1982).
3. J. M. Thomas, J. Klinkowski, S. Ramdas, B. K. Hunter, and D. Tennakoon, *Chem. Phys. Lett.* **102** Nos. 2, 3, 158 (1983).
4. (a) J. R. MacDowell, U. S. Pat. No. 3445 252, May (1969); (b) C. T. Li, U.S. Pat. No. 4073655.
5. C. N. Fenner, *Am. J. Sci.* **36,** 331 (1913).
6. M. A. Carpenter and M. Wennemer, *Am. Min.* **70,** 517 (1985).
7. O. W. Florke, *Ber. Keram. Ges.* **32,** 369 (1955).
8. V. G. Hill and R. Roy, *Trans. Br. Ceram. Soc.* **57,** 496 (1958).
9. M. O'Keefe and B. G. Hyde, *Acta. Crystallogr. Sect. B* **32,** 2923 (1976).
10. A. F. Wright and A. J. Leadbetter, *Philos. Mag.* **31,** 1391 (1975).
11. D. R. Peacor, *Z. Kristoallogr.* **138,** 274 (1973).
12. T. R. Welberry, G. L. Hua and R. L. Withers, *J. Appl. Cryst.* **22,** 87 (1989).
13. M. J. Buerger, *Am. Min.* **39,** 600 (1954).
14. M. J. Wilson, J. D. Russell and J. M. Tait, *Cent. Min. Pet.* **47,** 1 (1974).
15. J. V. Smith and C. S. Blackwell, *Nature* **303,** 233 (1983).
16. A. J. Perrota *et al., J. Am. Ceram. Soc.* **72,** 441 (1989).
17. M. A. Saltzberg *et al., J. Am. Ceram. Soc.* **75,** 89 (1992).
18. P. L. Gai-Boyes and J. M. Thomas, *Supercond. Rev.* **1,** 1 (1992), Gordon and Breach, Publishers.
19. J. M. Thomas, *Philos. Trans. R. Soc.* **33,** 173 (1990).
20. P. L. Gai and Q. Q. Chen, *Acta. Crystallogr. Sect. A* **38,** 741 (1982).
21. P. L. Gai-Boyes, J. M. Thomas, P. A. Wright, R. H. Jones, S. Natarajan, J. Chen, and R. Xu, *J. Phys. Chem.* **96,** 8206 (1992).
22. C. A. Fyfe, "Solid State NMR for Chemists," Chap. 7, CFC Press, Guelph (1983).
23. F. Liu *et al., Phys. Rev. Lett.* **70,** 2750 (1993).